PHASE SEPARATION IN A BINARY MIXTURE OF SEMIFLEXIBLE POLYMERS CONFINED IN A REPULSIVE SPHERE

Andrey Milchev[1,*], Sergei A. Egorov[2], and Kurt Binder[3]

[1*] *Institute of Physical Chemistry, Bulgarian Academy of Sciences, 1113 Sofia, Bulgaria, email: milchev@ipc.bas.bg*

[2] *Department of Chemistry, University of Virginia, Charlottesville, Virginia 22901, USA and*

[3] *Institut für Physik, Johannes Gutenberg-Universität Mainz, Staudinger Weg 9, D-55099 Mainz, Germany*

Abstract

Lyotropic solutions containing two types of semiflexible macromolecules in spherical confinement are studied by Molecular Dynamics simulations and Density Functional Theory, using a coarse-grained model. The case of strong stiffness disparity between both types of polymers is treated, and for simplicity we take the contour lengths of both types of polymers to be equal. Only sphere radii larger than this contour length are considered, so many chains can be packed inside the sphere, even when the chains are stretched out in a nematic state. For the chosen polymer solution, in the bulk one finds with increasing monomer concentration a transition from an isotropic phase through an isotropic- nematic two-phase region to a homogeneous nematic phase to which both constituents contribute. In the corresponding confined systems, there is an interplay between these phase transitions and surface enrichment of one component (typically, but not always, the stiffer one). In rather dilute confined solutions, the main effect of the surfaces is that the random orientation of the end-to-end vectors of the stiff chains is perturbed in a surface shell whose thickness is roughly the contour length. In more concentrated systems, a thin layer of wall- attached stiff chains is observed in addition, while (for equal mole fraction of both constituents) the stiffer component can also form an almost cylindrical domain with a bipolar orientational order, surrounded in the remainder of the sphere by the less stiff component. Topological defects in the nematic order can be identified, similar to the case where a single type of semiflexible polymer is confined in a sphere. The radial profiles of monomer concentrations and of various order parameters are compared to analogous data near planar and cylindrical repulsive walls, to provide a comprehensive picture of confinement effects on such polymer solutions.

I. INTRODUCTION

Confinement of biopolymers by cell membranes plays a great role for many phenomena occurring in living matter[1], examples include packaging of double-stranded (ds) DNA in bacteriophage capsids[2,3], storage of chromatin in the nucleus of cells, organization of actin filaments confined by cells[4], etc. Related problems occur in applications where capsules (in the size range from 100 nm to 10 micrometer diameter) transport polymeric molecules to achieve specific actions, such as drug delivery[5,6] in medicine or agriculture. There the release of the drug may be triggered in various

ways (change in the pH value of the ambient solution, irradiation, etc.), but this aspect is not further considered here. Here we rather focus on the problem that there may be the need to consider several kinds of (bio-)polymers together confined in such a capsule. This case has also occasionally been considered by targeted experiments, where, e.g., ds DNA and actin confined in spherical vesicles were studied[7].

A characteristic aspect of many polymers and biopolymers in particular is that chain stiffness plays an important role: the persistence length ℓ_p that characterizes chain stiffness may vary within the range of a few nanometers (e.g., single stranded DNA[8]) to many micrometers (e.g., rod-like viruses[9]). While stiff macromolecules in bulk solution under good solvent conditions show interesting cooperative phenomena such as long range ordered liquid crystalline structures[10–13], it has been found that in spherical confinement such structures are severely distorted and the order is disrupted by topological defects[14–16]. Particularly interesting structures have been found for the problem of very long single ds-DNA chains packed in spheres modelling bacteriophage capsids[2,3,17–22]. In the spirit of "molecular mechanics models", DNA is described as an elastic wire which can be packed into the sphere in the form f concentric spools or coaxial spools[17,18], but also folded or twisted toroids have been found for other capsid shapes[17,18]. Theory[19–22], such as work using the selfconsistent field theory[20], has clarified the various "phases" of single wormlike chains confined in spheres of radius R in terms of the parameters ℓ_p/R, where ℓ_p is the persistence length, and the density of persistent segments in the sphere. Also orderings exhibiting Hopf fibrations have been found[20], in addition to the coaxial spool state and the isotropic phase at low enough density.

When one considers different types of semiflexible polymers where the persistence length is much larger than the linear dimension of a monomeric repeat unit, confined in a capsule, enthalpic forces will typically cause very strong segregation: aggregates of the minority component appear on the background of the solution containing the majority component[23]. However, this case shall not be considered further here: often it may be preferable to have a situation where both components exhibit partial or full miscibility in a common solvent[7,24–27]. Yet, even in a common solvent which is a very good solvent for both species, entropically driven unmixing may occur, caused by a disparity of the effective thickness d of the rod-like polymers[1,25], or by mismatch of their contour lengths L, or stiffness[24]. Note that d is in the range of $0.5\,nm$ to $1.5nm$ for most synthetic semiflexible polymers[11,13,28], while for ds DNA in aqueous solution one has $2\,nm < d < 20\,nm$ (depending on salt concentration[29]), and $d = 8\,nm$ for actin[7]. Also for blends formed from rather flexible chains it has been found that a slight stiffness disparity causes a tendency in favor of surface segregation of the stiffer component[30]. Finally, we also draw attention to the entropically driven separation between just two identical chains confined in a narrow cylindrical tube[31,32].

Here we shall focus on the effect of spherical confinement on a mixture of semiflexible polymers with stiffness disparity only; the bulk behavior of such systems has been studied earlier by some of us with Molecular Dynamics (MD) simulations and density functional theory (DFT) for a coarse-grained model[26,27]. We shall study the interplay of surface enrichment of one component (driven only by entropy, no enthalpically driven adsorption being considered) with the distortion of nematic order, and compare to the behavior of corresponding confined solutions containing a single kind of semiflexible polymer.

Section II briefly characterizes the studied model and summarizes the essentials of the DFT and MD methodologies. Section III presents numerical results for dilute and semidilute solutions which in the bulk still occur in the isotropic phase, and compares the results with corresponding results for confinement in cylindrical tubes or between planar repulsive walls. Section IV then discusses denser systems, where in the bulk the presence of nematic order would matter, studying the deformation of this order by spherical geometry and the interplay with the entropy of mixing for the two species. For one-component systems[14,15] the role of topological defects on the nematic order has already been elucidated; here we extend this work to consider the interplay of these defect structures with surface enrichment of the stiffer component. Finally Section V summarizes our conclusions.

II. MODEL AND METHODS

Following previous work[14,15], we describe the stiff polymers as a sequence of N spherical beads of diameter σ and a bending potential $U_{bend}(\theta_{ijk})$ depending on the bond angle θ_{ijk},

$$U_{bend}(\theta_{ijk}) = \epsilon_{bend}(1 - \cos(\theta_{ijk})). \tag{1}$$

Here i, j, k label the coordinates $\vec{r}_i$, $\vec{r}_j$ and $\vec{r}_k$ of three subsequent beads along the chain, i.e., the bond vectors are $\vec{a}_j = \vec{r}_j - \vec{r}_i$ and $\vec{a}_k = \vec{r}_k - \vec{r}_j$, θ_{ijk} being the angle between two subsequent bond vectors. For DFT, the chain molecules are treated as tangent hard sphere chains so the bond length ℓ_b is precisely equal to the bead diameter σ (which is chosen as the length unit). For MD, it is more convenient to use the standard Kremer-Grest[33] bead-spring model (with a scale $\epsilon = k_BT = 1$ for the repulsive bead-bead potential). In this model $\ell_b = 0.97$, and $\sigma = 1$ can also be used as the effective chain diameter D in both models. The contour length then is $L = (N-1)\ell_b$, and the persistence length of these models can be computed from

$$\ell_p/\ell_b = -1/\ln\langle\cos(\theta_{ijk})\rangle \approx 2/\langle\theta_{ijk}^2\rangle. \tag{2}$$

Note that in very dilute solution we also have $\ell_p/\ell_b = \kappa = \epsilon_{bend}/(k_BT)$ and in Eq.2 in the second step we have assumed that $\kappa \gg 1$, so that only small angles θ_{ijk} in Eqs.1,2 matter.

In less dilute solutions, however, where a transition to the nematic phase has occurred[10–13], the persistence length measured from Eq.2 exceeds κ and depends on the density ρ of the monomeric units (as well as on κ and N)[34]. The order parameter S of the nematic phase is defined as the largest eigenvector of the traceless tensor

$$Q^{\alpha\beta} = (3\langle\vec{u}_i^{\alpha}\vec{u}_i^{\beta}\rangle - 1)/2. \tag{3}$$

The averages $\langle\ldots\rangle$ in Eqs.(2,3) are taken over all bonds and all chains of a particular kind A, B, when we have two different species of semiflexible polymers in solution. While we then need to distinguish κ_A, κ_B, ℓ_p^A, ℓ_p^B and

S_A, S_B, the model is chosen such that there is neither a distinction with respect to bond length ($\ell_b^A = \ell_b^B$) nor repulsive interaction between monomeric units ($\epsilon_A = \epsilon_B$, $\sigma_A = \sigma_B$). When we also assume identical chain lengths ($N_A = N_B = N$), stiffness disparity is the only distinctive feature of the two species.

Even if the stiffness disparity is very large (consider, e.g., the case $N = 32$, $\kappa_A = 24$, $\kappa_B = 128$), conformations of one type of a chain (as measured, e.g., by the mean square end-to-end distance $\langle R_e^2 \rangle$, or gyration distance $\langle R_g^2 \rangle$, etc.) remain essentially unperturbed by the presence of the other type of chain in the isotropic phase[1,27].

This is no longer true in nematic phases containing two types of chains with different stiffness: there occurs a mismatch in chain packing between the two types of chains, and the order parameters S_A, S_B and end-to-end radii $\langle R_e^2 \rangle_A, \langle R_e^2 \rangle_B$, etc., in the mixture differ from their counterparts in the respective pure phases. For large enough stiffness disparity even a phase separation into two coexisting nematic phases (one A-rich and the other B-rich) occurs[26]. In the following we restrict attention to the region of parameters where in the bulk there still occurs miscibility between A and B also in the nematic phase.

As described in previous work for confined single component systems of semiflexible polymers[14,15,35], we carry out standard MD simulations[36] using two choices for the radius R of the rigid spheres confining the polymers, $R = 35$ and $R = 70$, the repulsive potential acting from the sphere surfaces is chosen to have the same form as the monomer-monomer repulsion, also with the same range $\sigma = 1$ and strength $\epsilon = 1$. We use Graphics Processing Units (GPU's) and apply the HOOMD Blue software[37,38]. Fig.1 presents typical snapshot pictures of equilibrated configurations that will be analyzed in the next sections. More details on the simulation methods can be found also in Refs.[14,15,26,36].

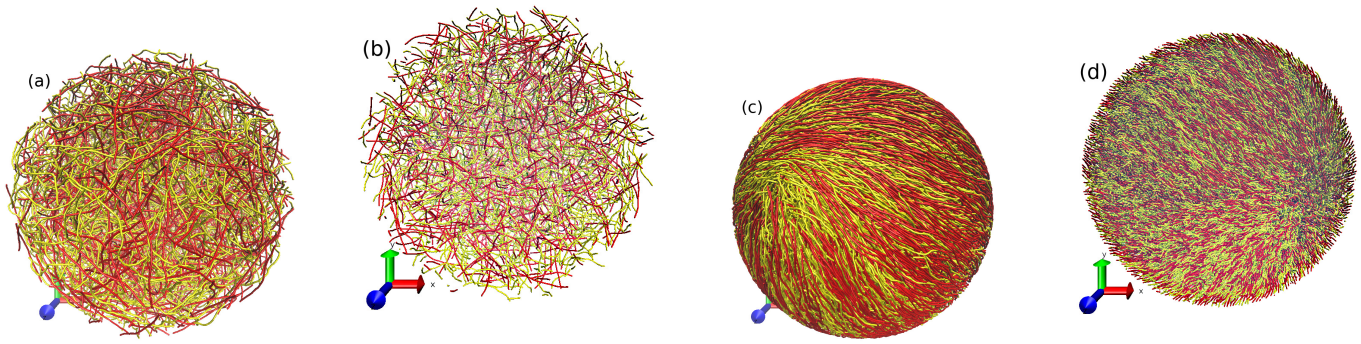

FIG. 1: Snapshot configurations of binary mixtures ($\kappa_A = 24$, $\kappa_B = 128$, $N_A = N_B = 32$, mole fraction $X_A = 0.5$) confined in a sphere of radius $R = 70$. Panels a,b refer to monomer density $\rho = 0.06$ and panels c,d to $\rho = 0.42$, respectively. The less stiff A-chains are displayed in yellow, the stiffer B-chains in red. Panels a, c are side views, while panels b, d show cross-sections through the sphere center. For the low density one has an isotropic mixture with reduced local density close to the sphere surface; for $\rho = 0.42$ one has a mixed nematic phase, strongly distorted by the splay deformations imposed by the confinement. From the side view (panel c) one can see that there occurs significant surface enrichment of the stiffer component, and one of the topological defects occurring for a bipolar configuration can also be recognized, with less stiff chains enriched near the defect.

For the DFT calculations, confinement was effected by spheres with hard walls, and in principle, one would need to minimize a free energy functional depending on the molecular density $\rho_{mol}(\vec{r}, \omega)$, where ω stands for all the variables describing the molecular orientation. Following the treatment of Fynewever and Yethiraj[39,40], the orientational

degrees of freedom of individual bond vectors are only indirectly considered by means of the effective excluded volume interaction $V_{exc}^{\alpha,\beta}(\omega,\omega')$ between a chain of type α and a chain of type β (with $\alpha,\beta = A,B$). The dependence on ω and ω' is thus reduced to a dependence on a single variable, the relative angle between the orientation vectors of the two chains. These interactions were computed in the context of the studies on the behavior of bulk mixtures[26,39] and are used here again, we assume that these interactions do not change when the two semiflexible polymers are close to the confining surface, although then the typical chain conformations may differ.

While in the bulk it was assumed that $\rho_{mol}(\vec{r},\omega)$ can be factorized into $\rho_{mol}f(\omega)$, where ρ_{mol} is just the average molecular density so any spatial dependence was neglected, for spherical confinement we need to allow for a dependence on the radial distance r from the center of the sphere,

$$\rho_{mol,\alpha}(\vec{r},\omega) = \rho_{mol,\alpha}(r,\omega) = \rho_{iso,\alpha}(r) f_\alpha(r,\omega) \tag{4}$$

We assume here that $f_\alpha(r,\omega)$ is normalized to unity, and that far from the wall the state of the solution is the isotropic phase, irrespective of A or B. Note that the $f_\alpha(r,\omega)$ needs to be interpreted as the orientational distribution function of a chain (averaged over all bond vector orientations of this chain) whose center of mass coordinate is at a distance r from the sphere center. Apart from the need to distinguish the species A and B, the treatment is the same as for the confinement of a single type of semiflexible polymers, used successfully earlier[35,42]. A particular bonus of DFT is the fact that it yields explicitly the free energy of the considered model system, which then can be split into a bulk term and a surface correction[35],

$$F_{tot} = \frac{4\pi R^3}{3} f_{bulk} + 4\pi R^2\, \gamma(R) \tag{5}$$

following[35], who noted that it is necessary to allow for a dependence of the surface tension $\gamma(R)$ on the sphere radius R. Of course, both the bulk free energy and $\gamma(R)$ will depend on the mole fraction X_B as well.

For the DFT calculations we did focus on the case $N_A = N_B = 32$ but for simplicity considered not extremely stiff chains, namely, we focused only on $\kappa_A = 8$ and $\kappa_B = 32$. We choose two densities, $\rho = 0.06$ and 0.2, in the isotropic region. In this case, several radii $R = 25$, 35, 50 and 75 were studied as well as the planar wall case ($R \to \infty$).

III. NUMERICAL RESULTS FOR THE CASE WHERE THE BULK IS STILL AN ISOTROPIC SOLUTION

A. DFT RESULTS

Already for solutions of a single kind of semiflexible polymers it has been found[35] that the surface tension $\gamma(R)$ for dilute solutions confined by repulsive walls is small and positive (typically $0.01 < \gamma(R)/k_BT < 0.10$) but it exhibits a nontrivial dependence on both chain length N and stiffness κ for the considered monomer densities. When we extend

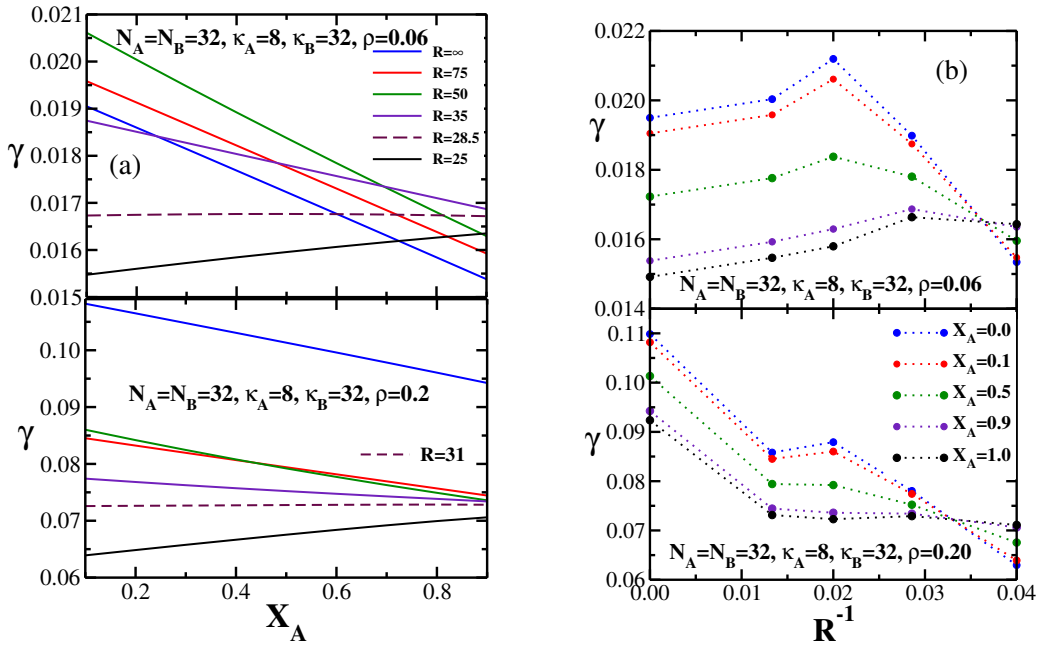

FIG. 2: a) Surface tension $\gamma(R, X_A)$ plotted vs. X_A for average density $\rho = 0.06$ (upper part) and $\rho = 0.20$ (lower part). Both the case of a planar wall ($R = \infty$) and five choices of R are included, as indicated. Dashed lines denote the cases $\gamma(R^*) = const.$ b) Variation of γ with inverse sphere radius R^{-1} for several values of X_A. Dotted lines are guides to the eye only.

these studies to binary mixtures, Fig.2, we again find that the approach of $\gamma(R, X_B)$ to the result for a planar wall ($\gamma(R = \infty, X_B)$ is a non-monotonic function of R. But for any fixed value of R the dependence of $\gamma(R, X_B)$ on X_B is almost perfectly linear. A strictly linear behavior can be expected if we have ideal mixing conditions with respect to both A and B in the bulk and near the surface[41].

$$\gamma(R, X_A) = \gamma_A(R)X_A + \gamma_B(R)(1 - X_A). \tag{6}$$

For $R = 25$ the A-chains have a larger surface tension than the B-chains while for larger R the situation is reversed so the slope of γ with X_A has a different sign, Fig.2a. As a consequence, between $R = 25$ and $R = 35$ a radius must occur, where $\gamma(X_A)$ is essentially horizontal: this shows up as a common intersection point of the dotted lines in Fig.2b. But this particular radius does depend on the chosen density somewhat and hence it is not the same for the two densities shown in Fig.2b. While for the bulk solutions[26] at the densities shown here ideal mixing indeed is expected, this is not obvious at the surface. A particularly interesting case occurs for radii R^* when $\gamma_A(R^*) = \gamma_B(R^*)$, since then the above linear relation implies that $\gamma(R^*, X_A)$ is completely independent of X_A. While for an ideal mixture of point particles one would then expect that radial profiles of the volume fraction $\phi_A(r) = \rho_A(r)/(\rho_A(r) + \rho_B(r))$ are perfectly flat and structureless, this is not the case here. For polymers there occur nontrivial correlations of the monomeric densities $\rho_A(r)$, $\rho_B(r)$ even in the dilute limit due to the structural correlation along the contours of the chains: for $N = 32$ and $\kappa = 8$, the root mean square end-to-end distance is about 19.25, according to the Kratky-Porod wormlike chain model, while for $\kappa = 32$ it is about 26.7. Now one can expect that the densities $\rho_A(r)$, $\rho_B(r)$

near a wall are strongly affected up to the distance of one half of these values since the orientations of the end-to-end vectors are constrained not to cross the wall. Since these end-to-end distances differ for the two types of chains, a nontrivial behavior arises, and also for $R = R^*$ no special behavior of these densities is seen, Fig.3c. We find here a nonmonotonic behavior of the local mole fractions $\phi_A(r)$, $\phi_B(r)$, which cross each other twice, since very close to the wall the density of B-monomers is enhanced but over a broad adjacent region the density of A-monomers is enhanced while in the center B dominates again. The distances between the resulting crossing points where $\phi_A(r) = \phi_B(r)$ for the average composition $X_A = 0.5$, depend in a subtle way on the difference between $\gamma_A(R)$ and $\gamma_B(R)$. Radial profiles, Fig.3, indicate that for $\rho = 0.20$ a pronounced surface enrichment of the less stiff component (A) takes place. Since the total volume fraction X_A as well as the average density in the sphere are strictly fixed, there must then

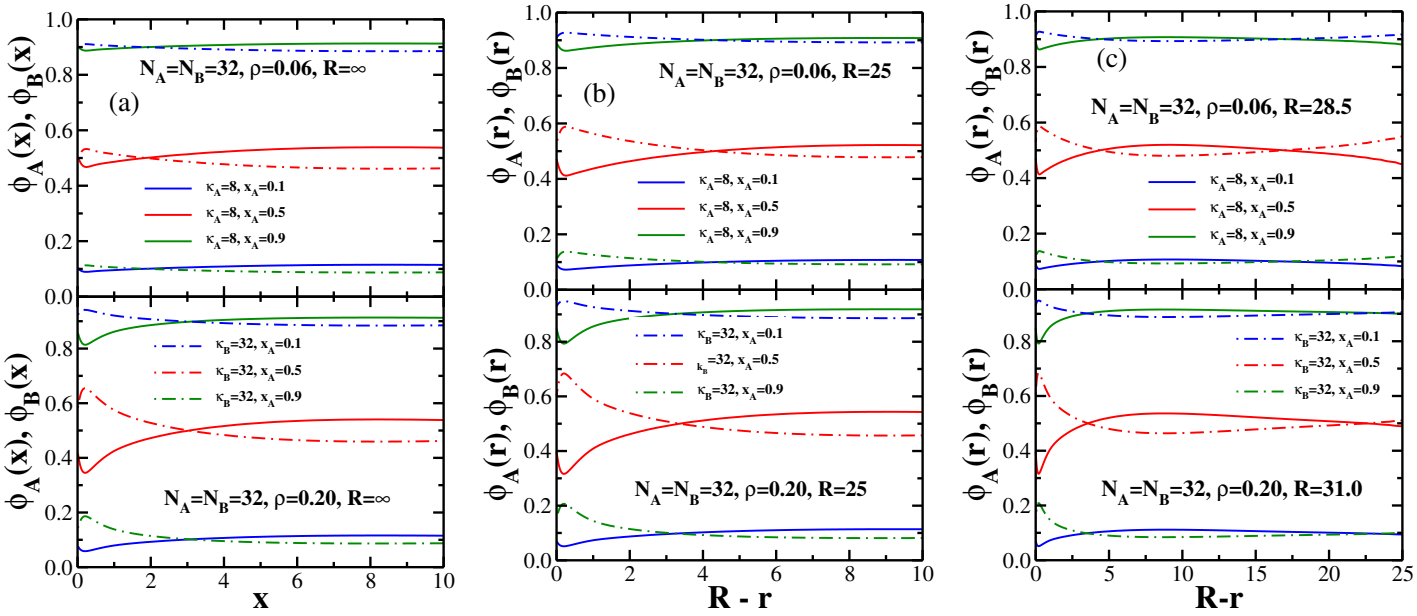

FIG. 3: a) Plot of the local monomer fractions $\phi_A(x)$, $\phi_B(x)$ as a function of distance x from a planar wall, for a density $\rho = 0.06$ (upper panel) and $\rho = 0.20$ (lower panel). In each panel three choices of volume fraction $X_A = 0.1, 0.5, 0.9$ are included, and the two curves for each case are simply related via $\phi_A(x) + \phi_B(x) = 1$. b) Plot of the local molar fractions $\phi_A(r)$, $\phi_B(r)$ versus the radial distance $R - r$ for a sphere with $R = 25$, for a density $\rho = 0.06$ (upper panel) and $\rho = 0.20$ (lower panel). In each panel three choices of volume fraction $X_A = 0.1$, 0.5 and 0.9 are included. c) The same as in b) but for the special radii $R^* = 28.5$ and $R^* = 30.10$ for which $\gamma(X_B) = const.$

occur a depletion of the local mole fraction $\phi_A(r)$ in the center of the sphere. For the case of planar surfaces, this depletion also occurs for distances exceeding 5σ from the wall, since actually the calculation does not deal with a semi-infinite system, but rather with a thin film confined between two planar walls a distance $L = 40\sigma$ apart, as chosen for the one-component systems[42]. However, the variation of the local total density $\rho(r)$ with the distance r from the confining surface indicates, Fig.4, that the surface tension reflects mostly the free energy cost due to the local inhomogeneity of the total density near the surface; the local composition obviously plays only a minor role. It is seen that the stiffer chains for $R = 25$ and $\rho = 0.2$ approach their maximal density, which occurs far from the surface, by a slow monotonic increase while the less stiff ones show a density maximum at a distance of about 0.6σ from the wall, followed by a minimum at about twice this distance. We interpret this behavior as a precursor of the

well-known layering structure that prevails near hard walls for larger monomer densities. For $R = 50$ (not shown here) this maximum is also present, though slightly less pronounced, while for the planar wall no longer a maximum is found but only a shoulder.

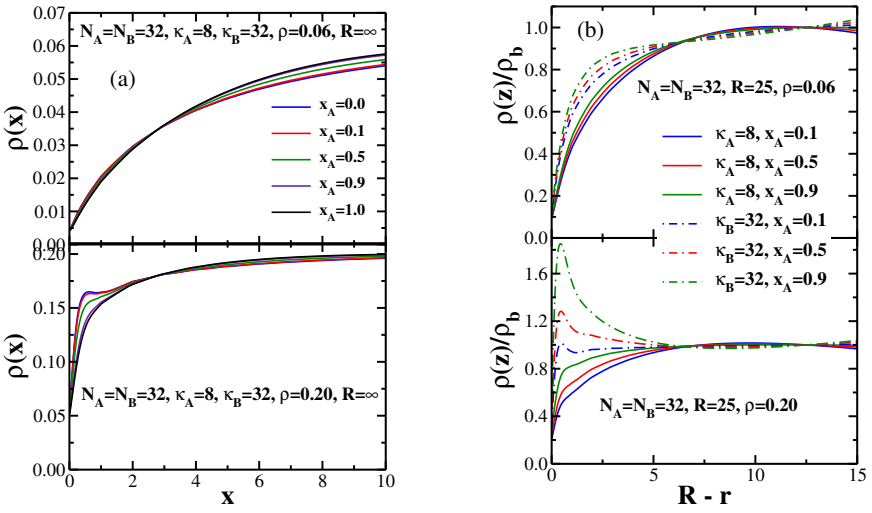

FIG. 4: a) Plot of the local density $\rho(x)$ as a function of distance x from a hard wall, for $\rho = 0.6$ (upper panel) and 0.20 (lower panel). 5 choices of X_A are included, as indicated. b) Plot of the local density $\rho(r)$ versus $R - r$ for a sphere with $R = 25$, for a density $\rho = 0.06$ (upper panel) and 0.20 (lower panel). 5 choices of X_A are included, as indicated.

We remind the reader that in the present DFT study a single chain length $N_A = N_B = N = 32$ is used, chosen such that for all considered sphere radii in the dilute case the chains can fit into the sphere without significant deformation of the conformations they typically have in the bulk systems in equilibrium. The dramatic changes of the conformational behavior of confined semiflexible polymers that occur when N exceeds the sphere diameter are very interesting but will be not studied here as far as for single confined chains extensive work on this problem can be found in the literature[21,44,45].

One can also ask how individual monomers of the chains are distributed, such as monomers at the chain ends (the index i labeling the monomeric units along the chain contour takes the values $i = 1$ and $i = N$) or in the middle of the chain ($i = N/2$ or $i = 1 + N/2$, recall that N is chosen always even here). Fig.5a shows that end-monomers of the less stiff chains are strongly enriched near the surface, for the stiffer chains, end-monomers are depleted near the surface for $\rho = 0.06$ but slightly enhanced for $\rho = 0.20$. Mid-monomers, on the other hand, show a more complex behavior which is less straightforward to interpret: there is a delicate interplay of chain configurational entropy with the repulsion due to the confining sphere and entropy of mixing in the binary system. The distance of the maximum of the mid-monomer density from the surface corresponds roughly to 50% of the end-to-end distance of the chains. One can estimate the latter for our choices of stiffness and chain length rather reliably even with the simple Kratky-Porod wormlike chain model[43]. For chains at such a distance from the surface, the latter does not constrain their conformation any longer, therefore, there is an entropic driving force to "push" chains which would be closer to the surface just outside of this range where the chains can directly "feel" the constraining effect of the surface on their conformation.

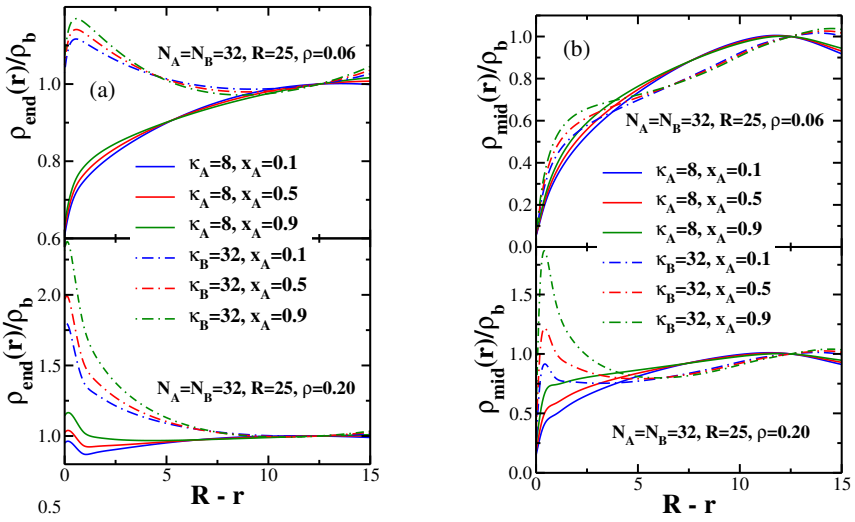

FIG. 5: a) Plot of the local density $\rho_{end}(r)/\rho_b$, where ρ_b is the density in the center of the sphere of radius $R = 25$, plotted vs. $R - r$, for the same case as in Fig.3b. b)Same as a), but for the mid-monomers.

B. Results from MD simulations

Typical results for the density profiles of A-monomers, B-monomers and the profile of one half of the total density are shown in Fig.6 for the average density $\rho = 0.12$ in the system, focusing on the case $N_A = N_B = 32$ and $X_B = 0.5$ again, but choosing rather stiff chains, $\kappa_A = 24$ and $\kappa_B = 128$. We compare here the case of a planar wall (panel a), a sphere of radius $R = 35$ (b), a sphere of radius $R = 70$ (c), and a cylinder of radius $R = 70$ (d). To make the comparison of the wall effects easier, we have chosen the origin of the abscissa always right at the wall, and choose the same scale for the abscissa (showing the region up to a distance of 35σ from the wall in all cases, to obtain a clear view of the behavior near the surfaces.

It is clearly seen that the local total density is essentially zero very close to the surfaces, and increases for the planar wall to the bulk monomer density within a distance of a few monomer diameters. The full bulk value for the planar wall is reached at a distance of about 10σ (note that $\rho_{bulk} = 0.126$ rather than the average value $\rho = 0.120$ here, since again the total number of the monomeric units in the slit pore is strictly fixed, and so the monomer depletion near the walls must be compensated by a slight enhancement of the density in the bulk).

In contrast, the densities of A- and B-monomers behave differently: for the stiffer B-chains, a first plateau is reached already at a distance of 1 to 2 units, and their density stays slightly below the value $0.063 = \rho_{bulk}/2$ reached at a distance of about $x_{bulk,B} = 29$ units from the wall. In the range of distances less than x_{cross}, defined from the condition $\rho_A(x = x_{cross}) = \rho_B(x = x_{cross})$, with $x_{cross} = 10$ in this case, it even happens that $\rho_A(x) > \rho_{bulk}/2$. ρ_{bulk} for the A-monomers is also reached for a distance of about $x_{bulk,A} = 29$. For lyotropic solutions of a single kind of semiflexible polymers[42], the approach of the density to its bulk value for densities $\rho_{bulk} < 0.2$ is always monotonic, increasing with x and reaching ρ_{bulk} at $x_{bulk} = 15$, very similar to the behavior of the profile of the total density here.

The numbers $x_{bulk}, x_{bulk,A}$ and $x_{bulk,B}$ can be interpreted tentatively in terms of the end-to-end distance of about

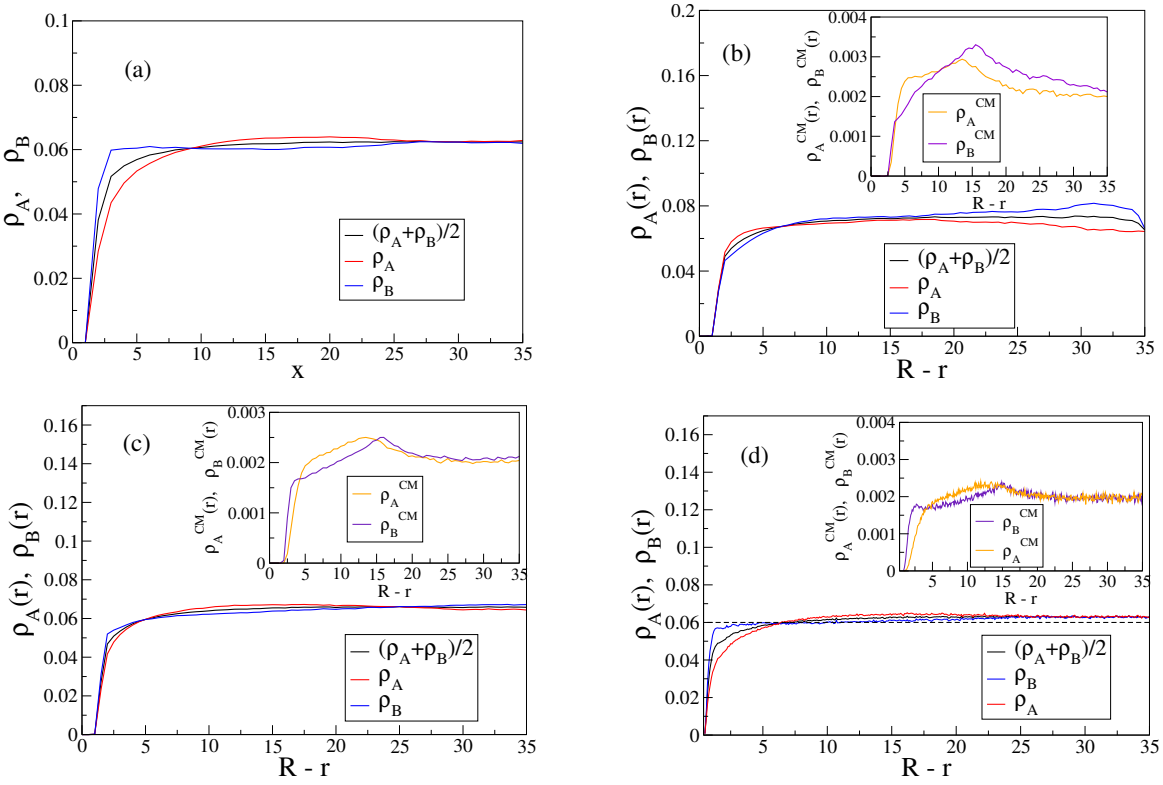

FIG. 6: a) Profiles $\rho_A(x)$, $\rho_B(x)$ of the densities of A-monomers and B-monomers as a function of the distance x from a planar repulsive wall for the case $N_A = N_B = 32, \kappa_A = 24$, $\kappa_B = 128$, at a total density $\rho = 0.12$ in a slit of width $D = 128$ and mole faction $X_B = 0.5$. For comparison the profile of half the total density, $\rho(x)/2 = (\rho_A(x) + \rho_B(x))/2$ is also included. b) Same as a) but for a repulsive sphere with radius $R = 35$. inset shows density profiles of the center of mass positions r_A^{CM}, r_B^{CM} . c) Same as b), but for a repulsive sphere with $R = 70$. d) Same as a)-c), but for a cylindrical pore with a repulsive surface and cylinder radius $R = 70$.

28.9 of the stiffer chains, which are almost rodlike. For such stiff chains, the conformation is already affected by the wall if the center of mass is at a distance $x_{CM,B}$ less than half the chain end-to-end distance from the wall, since then the orientational degrees of freedom of the end-to-end vector are already constrained. So B-chains are depleted somewhat from the region $x < x_{CM,B}$ and the density of A-chains is slightly enhanced there. Very close to the wall, however, both A-chains and B-chains need to be oriented parallel to the wall, then the more flexible chains with such a parallel orientation of the end-to-end vector are more constrained by the walls than the stiffer ones as they would lose more orientational entropy for their bond vectors. Hence one can understand that $\rho_B(x) > \rho_A(x)$ for $x < x_{cross}$. Clearly, such arguments can only be taken as a somewhat speculative interpretation of our findings, but obviously the packing of polymers in a mixture of chains with widely differing stiffness near a repulsive surface is controlled by a subtle competition of different entropic effects.

This "preference" of the repulsive surface for the stiffer chains is also seen in the case of the cylinder, and (to a lesser extent) for the sphere with $R = 70$ but not for the sphere with $R = 35$. As expected, if the radius of curvature of a confining surface is too small, a rod-like chain does not fit well to the surface; on the other hand, if R is very large, the behavior is hardly distinct from a planar surface.

These arguments are corroborated by the density distributions of the center of mass positions $\rho_{CM,A}(r), \rho_{CM,B}(r)$

shown in the insets of the various panels of Fig.6: in all cases peaks are found at distances of about half the end-to-end distance of the respective chains from the surface. The depression of the center of mass density for the B-chains close to the surface is most pronounced for the sphere with radius $R = 35$, again understandable by the argument that for a rodlike polymer with end-to-end distance 28.9 the largest misfit is experienced at the curved surface.

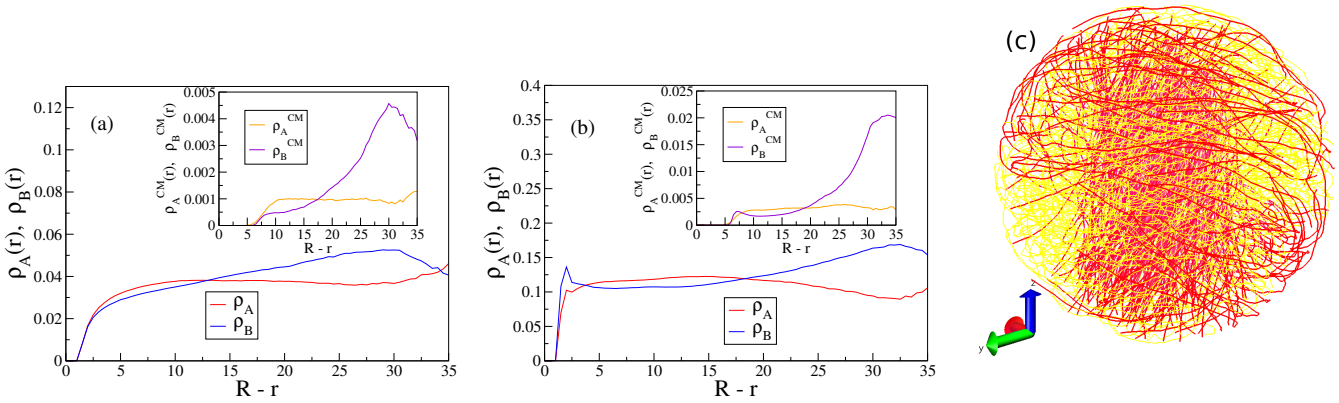

FIG. 7: Profiles $\rho_A(r)$ and $\rho_B(r)$ for the case $R = 35$, $\kappa_A = 24$, $\kappa_B = 128$, $N_A = N_B = 64$ and total densities (a) $\rho = 0.06$ and (b) 0.207. insets show the density profiles of the center of mass positions r_A^{CM} and r_B^{CM}. Panel c) shows a typical snapshot picture relating to case b), with A-chains displayed in yellow, and B-chains displayed in red.

It is important to recall that the behavior pointed out in Fig.6 and the accompanying discussion applies only in the parameter region for which the radius R of the sphere is larger than the end-to-end distance of the (almost rod-like) B-chains. For instance, if we instead consider the case $N_A = N_B = 64$ and still use $R = 35$, B-chains can still fit into the sphere without strong deformation of their typical conformations only if their center of mass position is close to the center of the sphere. In the corresponding density distributions, Fig.7, the consequences of this fact are borne out clearly. For very small average densities, such as $\rho = 0.06$ (Fig.7a) , the distribution of the center of mass of the stiff B-chains has a clear peak for radii $r < 10$, while for the less stiff A-chains the center of mass distribution is almost homogeneous up to $r = 25$. The preference of the stiff B-chains to stay near the sphere center shows up also in the monomer densities, $\rho_B(r) > \rho_A(r)$ for $r < 22$ at this average density (Fig.7a). At higher average densities, e.g., $\rho = 0.207$ (Fig.7b), the behavior is at first sight still similar, with the exception that now also a layer of surface-attached B-chains has formed in addition. This is also evident from the snapshot picture (Fig.7c), which reveals in addition that the B-chains that have their centers of mass near the sphere center are not randomly oriented but rather form a nematic "bundle" of chains more or less aligned parallel to each other. The still randomly oriented less stiff A-chains fill the remaining volume of the sphere almost homogeneously. The part of the "population" of B-chains in the surface layer take conformations almost similar to arcs of a circle. These conformations are reminiscent of the spiral-type structures found for single very long and very stiff chains (with $L \gg R$ and $\ell_p \gg R$) studied in the literature[21,44,45]. However, such structures are out of focus in the present investigation.

These considerations based on density distributions are well corroborated when we examine orientational order parameters of the bond vectors $\eta_A(r)$, $\eta_B(r)$ and end-to-end vectors $\eta_A^{EE}(r)$, $\eta_B^{EE}(r)$ defined as (we omit here indices

A, B for simplicity)

$$\eta(r) = (3\langle\cos^2(\theta(r)\rangle - 1)/2,\ \eta^{EE}(r) = (3(\langle\cos^2(\theta_{EE}(r))\rangle - 1)/2 \tag{7}$$

where $\theta(r)$ (or $\theta_{EE}(r)$, respectively) is the angle that a bond vector $\vec{u}_i(r)$ (or end-to-end-vector $\vec{R}_e(r)$, respectively) makes with the direction of the vector normal to the (spherical or planar) surface, and r is the distance of the center of the considered bond (i.e., the average of the positions of the monomers forming the bond vector), or the center of mass position of the considered chain, from the center of the sphere.

For the sphere, the quantity $R - r$ then is the distance from the surface, and this quantity can then be compared to the distance x from a planar wall, of course. But for the cylinder geometry, the situation is more complicated: the z-axis along the cylinder axis is a special direction, and the normal direction to the cylinder surface is another special direction. So the orientational order of both bond vectors and end-to-end vectors can be expected to be *biaxial*. In a separate study[46], the properties of single types of semiflexible polymers as well as their mixtures confined in cylinders have been already discussed whereby Eq.7 was also used albeit with a different meaning of the angles $\theta(r)$ and $\theta_{EE}(r)$, namely the angle between the bond and end-to-end vectors and the z-axis was considered. Consequently, then both quantities $\eta(r)$ and $\eta_{EE}(r)$ take positive values in the case when $r \to R$ while with the above definition Eq.7 for planar and spherical surfaces the order parameters tend to $-1/2$ when orientations parallel to the surface prevail. To avoid confusion, we have not included a discussion of orientational order parameters for cylinder geometry in the present paper.

Fig.8 then presents these orientational order parameters for the same choices of parameters as taken in Fig.6. Consistent with expectation, orientational order parameters η_A^{EE}, η_B^{EE} are zero (within statistical accuracy) whenever the distance from the surface exceeds one half of the corresponding end-to-end distance, the order parameters η_A, η_B become zero only when the distance exceeds the full end-to-end distance. Orientational correlations between the different bonds of a considered chain are thereby strong but no correlations exist between bonds of a chain near the surface and of bonds farther away, at these low densities.

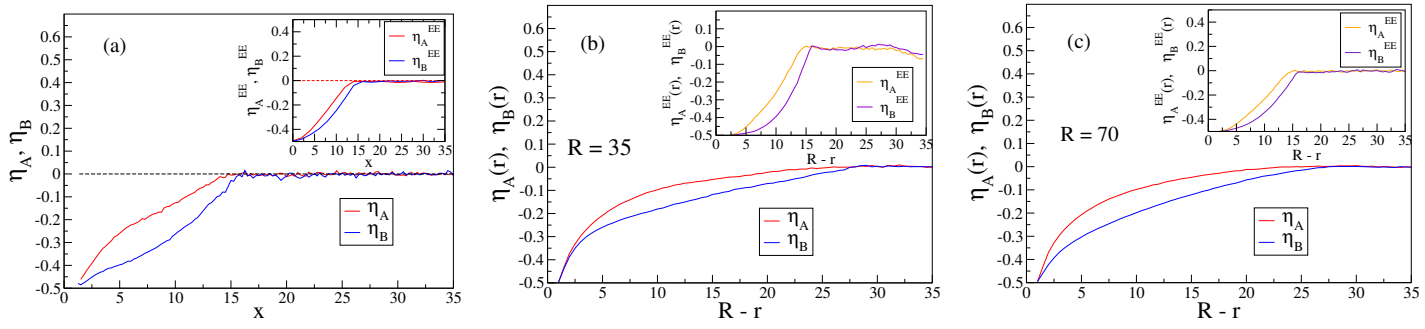

FIG. 8: a) Profiles of the orientational order parameters $\eta_A(x)$, $\eta_B(x)$ and $\eta_A^{EE}(x)$, $\eta_B^{EE}(x)$ (the latter shown in the inset) plotted as functions of the distance x from the planar repulsive wall, for the case $N_A = N_B = 32, \rho = 0.12, X_B = 0.5, \kappa_A = 24$, $\kappa_B = 128$. b) Profiles of the orientational order parameters $\eta_A(r)$, $\eta_B(r)$ and $\eta_A^{EE}(r)$, $\eta_B^{EE}(r)$ (insets) plotted as a function of the radial distance $R - r$ from the surface of a repulsive sphere, for the same parameters as in panel a) . c) Same as b), but for $R = 70$.

Closely related conclusions emerge when one studies the chain linear dimensions $\langle R_e^2 \rangle$ and $\langle R_g^2 \rangle$ for both types of chains. Components parallel and perpendicular to the radius vector (for spherical confinement) or to the surface normal (for planar confinement) differ from each other when the distance of the center of mass of the chain from the surface is less than $\sqrt{\langle R_e^2 \rangle}/2$, but are identical within statistical errors for larger distances, and agree with the corresponding bulk values. As it must be, parallel components of the end-to-end vector tend to zero for small distances (Fig.9a), but the sum $\langle R_e^2 \rangle_{||} + \langle R_e^2 \rangle_{\perp} = \langle R_e^2 \rangle$ stays approximately constant, independent of distance. So the chains at the considered low density are neither squeezed nor stretched by the surface effects, merely the chain orientations are affected. We have not included the case of $R = 70$ here as it is within errors indistinguishable from that of the planar surface. We emphasize that the behavior seen in Fig. 9a,b is not specific to the shown average density $\rho = 0.12$, but representative for a broad range of densities in the isotropic phase (we have checked this for $\rho = 0.06$, 0.09, 0.16 as well). However, close to the isotropic-nematic phase boundary (the two-phase coexistence region for $X_B = 1$ starts at about $\rho = 0.21$ and for $X_B = 0.5$ at $\rho = 0.23$) behavior no longer is similarly simple, the sharp boundary between the region affected by the surface and the bulk-like behavior is strongly rounded (Figs. 9c,d). This means that the local orientational order that occurs near the surface where the stiffer species is enriched both for spherical, cylindrical and planar confinement, causes nontrivial correlations over larger distances. The behavior now depends on the type of confinement distinctly: for planar geometry, an enrichment layer of B-chains close to the surface has formed at $\rho = 0.207$, Fig.9a, where the nematic order is close to saturation (Fig.10a,b). For the spherical geometry, we have a similar enrichment shell near the surface (Fig.10c) as for the planar case for the same density. However, the spherical

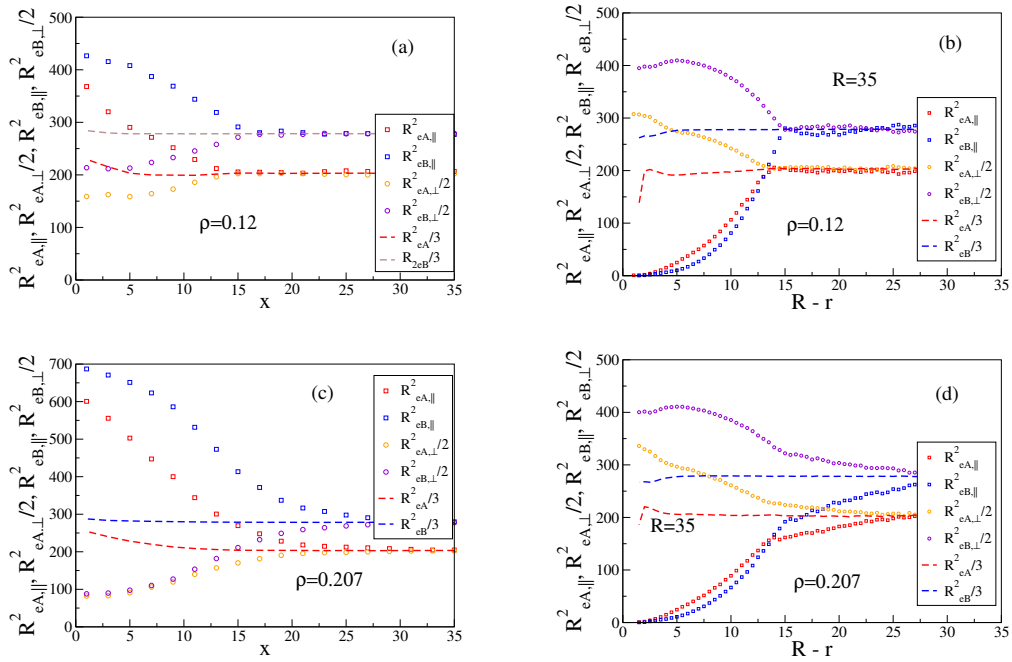

FIG. 9: a) Profiles of the parallel and perpendicular components of the mean square end-to-end distance of A-chains and B-chains near a planar surface plotted vs. x, for the same cases as in Fig.8. b) same as a), but for a sphere of radius $R = 35$. c) Same as a), but for a total density of $\rho = 0.207$. d) Same as b), but for a total density of $\rho = 0.207$.

geometry is in conflict with the nematic long range order, and snapshot pictures reveal that nematically ordered

clusters of B-chains form in the surface region, which do not have an uniform orientation of the local director, and are separated by interfacial regions rich in the less rigid A-chains (Fig.10d).

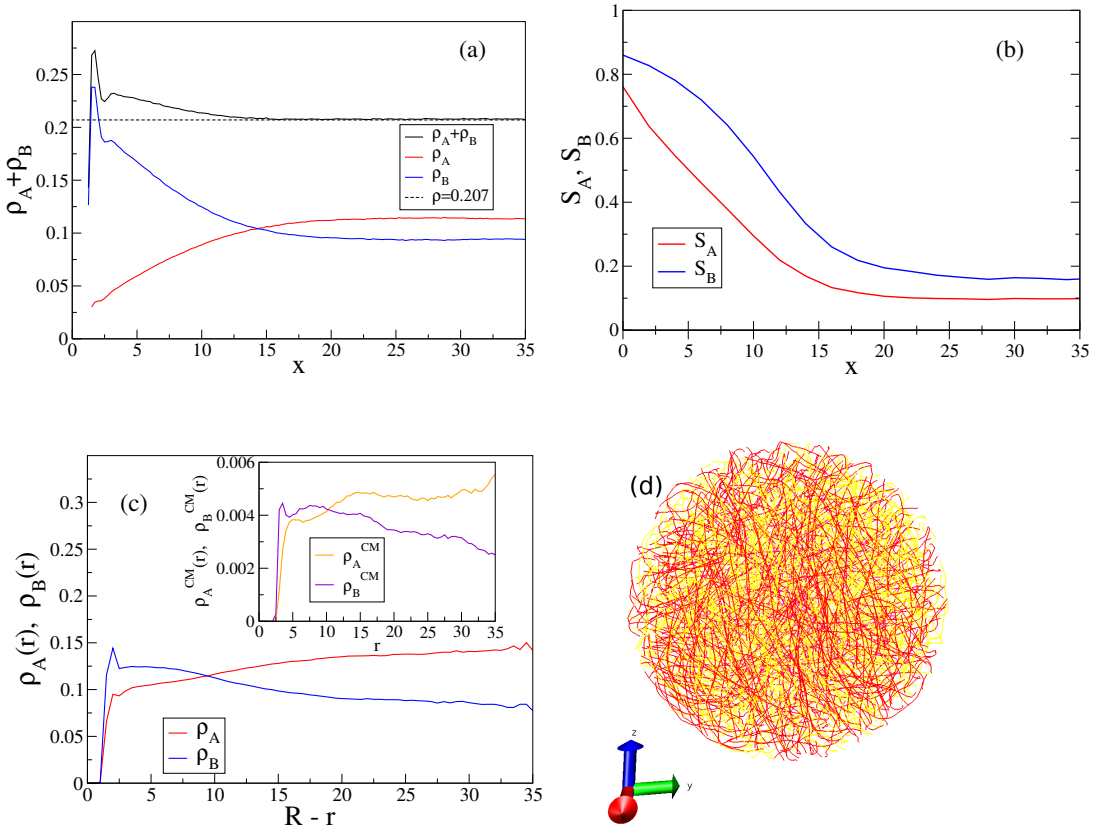

FIG. 10: a) Same as Fig.6a, but for a total density $\rho = 0.207$. b) Profiles of the nematic order parameters $S_A(x)$, $S_B(x)$ plotted vs. x, for the same system as in panel a). Note that the nonzero plateau values of order 0.1 to 0.2 in the center of the slit pore are artefacts due to finite size. c) Same as Fig.6c, but for a total density of $\rho = 0.207$. d) Snapshot of the system shown in panel c).

IV. MD RESULTS FOR CONFINED DENSE MIXTURES WHERE NEMATIC ORDER MATTERS IN THE BULK

The properties of the confined systems in the various geometries differ fundamentally from each other at still larger densities where in the bulk two-phase coexistence is encountered. The two-phase coexistence region for $X_B = 0.5$ and our stiffnesses is rather wide, it extends[46] from $\rho_i = 0.23$ to $\rho_n = 0.35$. For planar geometry, we would find domains with exactly those densities coexisting in the slit, if the slit thickness were macroscopically large, for all average densities in between these limits. However, for the present slit thickness of $D = 124$ a large part of this two-phase region is eliminated by the capillary nematization effect[47–54], studied previously for systems containing a single type of semiflexible polymer. For the present case, the nematic-isotropic interfaces of the nematically well ordered layers attached to both walls of the slit move towards one another with increasing density and annihilate each other: one then is left with a slit with almost uniform nematic order (Fig.11a,b). Thus it is clear that the region of

densities where two-phase coexistence with B-rich nematic domains adjacent to the walls and an A-rich (more or less isotropic) domain in between is clearly shifted, relative to the densities of the corresponding bulk two-phase region for $X_B = 0.5$. The nematic order of both components near the walls is enhanced (Fig.11b), although the density of A-chains near the walls is strongly depressed, Fig.11a, in favor of a strong surface enrichment of B-chains. This effect is strong enough to even cause an "overshoot" of the profile of $(\rho_A(x) + \rho_B(x))/2$ near the wall. The peak near the wall can clearly be interpreted as a precursor of the layering phenomenon that is found at still larger densities. At large distances from the wall, both $\rho_A(x)$ and $\rho_B(x)$ are independent of the distance from the walls, and $\rho_A(x) > \rho_B(x)$, since the average densities of both species in the slit must be equal for $X_B = 0.5$.

For the cylinder geometry, Fig.11c, the profile of $\rho_B(r)$ at comparable total densities shows two layering peaks already, and also the variation of $\rho_A(r)$, although strongly depressed near the surface, is nonmonotonic there. Again far from the wall we have $\rho_A(r) > \rho_B(r)$, due to the constraint that the average densities of both species in the cylinder must be equal to $\rho/2$. These properties require the occurrence of crossing points at r_{cross} (or x_{cross}, respectively) defined by $\rho_A(x_{cross}) = \rho_B(x_{cross})$, or $\rho_A(r_{cross}) = \rho_B(r_{cross})$, respectively. Note that these characteristic lengths are not in a straightforward way related to chain linear dimensions, since they are specific to our choice $X_B = 0.5$; by choosing X_B somewhat different from this value rather different crossing points could occur.

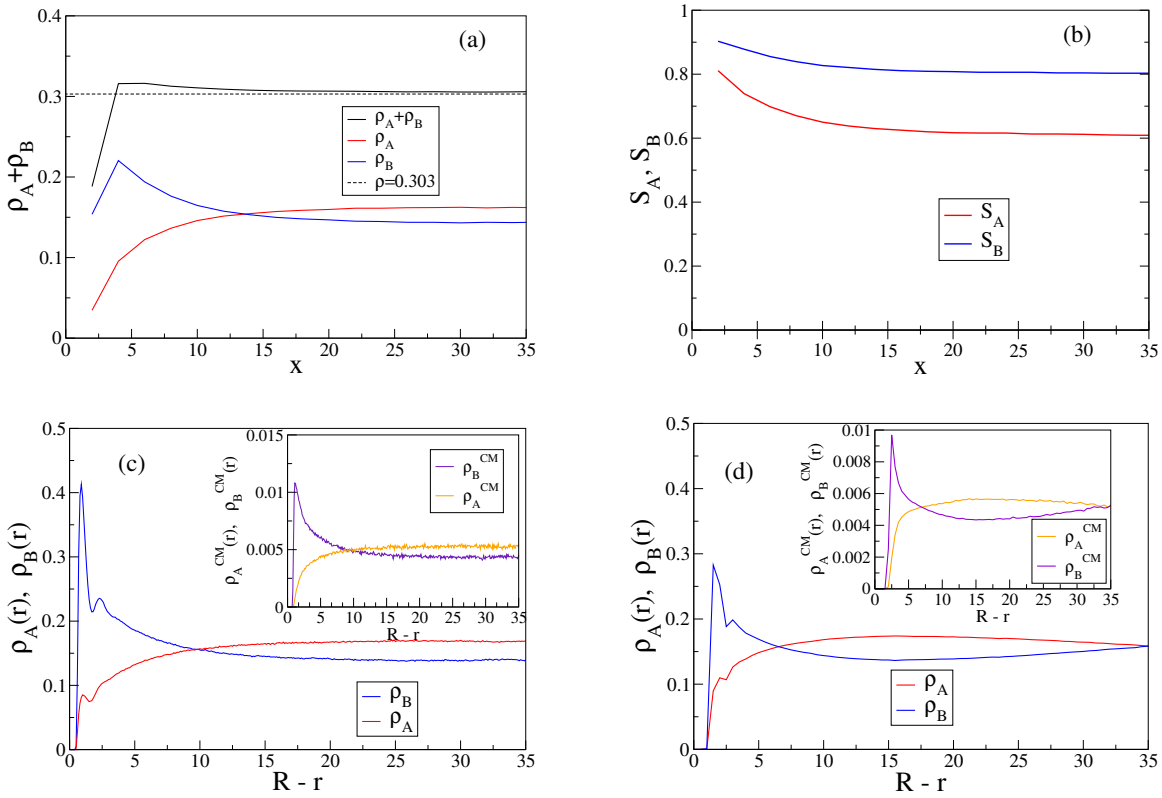

FIG. 11: Profiles $\rho_A(x)$, $\rho_B(x)$ of the densities of A- and B-monomers shown as a function of the distance x from a planar repulsive wall, for the case $\rho = 0.303$ and $X_B = 0.5$. b) Profiles of the nematic order parameters $S_A(x)$, $S_B(x)$, for the same case as in panel a). c) Profiles $\rho_A(r)$, $\rho_B(r)$ of the densities of A-monomers and B-monomers shown as a function of the distance $R - r$ from the wall of a cylinder with radius $R = 70$, for the case $\rho = 0.303$ and $X_B = 0.5$. d) Profiles $\rho_A(r)$, $\rho_B(r)$ for a repulsive sphere at $\rho = 0.303$ and $R = 70$ plotted vs. $R - r$. inset shows corresponding data base on the center of mass positions of the chains.

For the spheres with radius $R = 70$, remarkably, a second crossing point occurs far away from the surface, and the B-chains are enriched both near the surface and near the sphere center (Fig.11d). Chain linear dimensions (Fig.11e) indicate that the anisotropies in the orientation of the end-to-end vectors start near the sphere center and increase completely gradually as r tends to R. Of course, in this case a distorted nematic order, to which both types of chains contribute, exists everywhere in the sphere, the behavior is qualitatively similar to the case where a single type of semiflexible polymer is confined within a repulsive sphere[14,15].

When one studies the confinement at still larger densities, such as $\rho = 0.37$ and 0.42, where in the bulk a homogeneous nematic mixture occurs to which both types of chains then contribute, irrespective of their mole fractions X_A, X_B[26], the behavior of systems in planar and cylindrical confinement[46] is rather simple to understand: in both cases the nematic order parameters S_A, S_B are enhanced near the surface and decrease towards their bulk values that are reached at a distance of order 10 from the planar or cylindrical surface[46]. The local density of B-monomers is strongly enhanced near the surface (and the density of A-monomers is depleted), and clear evidence for layering is seen[46]. In neither of these cases does the confining surface cause "frustration" of the nematic order, unlike the case of spherical confinement (Fig.1c,d). Figs.12a,b show that nonuniform and nontrivial density profiles $\rho_A(r)$, $\rho_B(r)$ result for both $R = 35$ and $R = 70$ while the total density $\rho(r) = \rho_A(r) + \rho_B(r)$ shows a much weaker radial variation (apart from the layering effect that occurs only over a range of a few monomer diameters near $r = R$). Interestingly, also the center of mass profiles $\rho_B^{CM}(r)$ show pronounced peaks near the walls which indicate that part of the B-chains are in a wall-attached conformation, and the A-chains are enriched (in comparison with the B-chains) in a second spherical shell just underneath the wall-attached B-rich region.

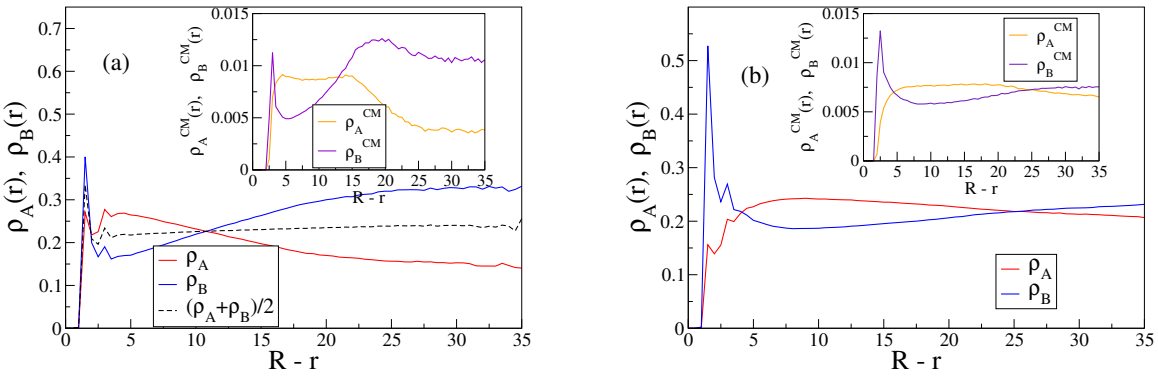

FIG. 12: Radial density profiles $\rho_A(r)$, $\rho_B(r)$, and $(\rho_A(r) + \rho_B(r))/2$ plotted versus $R - r$ and the case $N_A = N_B = 32, \kappa_A = 24, \kappa_B = 128, \rho = 0.42$ and $X_B = 0.5$. Two choices of R are shown, $R = 35$ (a) and $R = 70$. (b) insets show the corresponding profiles of the center of mass positions of the chains.

Particularly interesting structures due to spherical confinement of mixtures occur for still larger densities, such as $\rho = 0.63$ and $\rho = 0.70$, though we report these results only with the caveat that we cannot be sure whether these structures are true equilibrium states, or only long-lived metastable states. While the snapshot picture of the configuration for $R = 35$ reveals a structure (Fig.13a,b) where a large fraction of the stiffer B-chains form almost a cylinder inscribed to the sphere, reminiscent almost of two smectic cylindrical layers on top of each other, which leads

to a strong peak in their center of mass distribution at a distance of $r = 17$ from the sphere center, Fig.13c, for $R = 70$ the situation is completely different: density distributions resemble those found for $\rho = 0.42$ whereas at the surface interesting structures involving topological defects are identified, where now the less rigid A-chains are enriched near the core of these defects (Fig.13d).

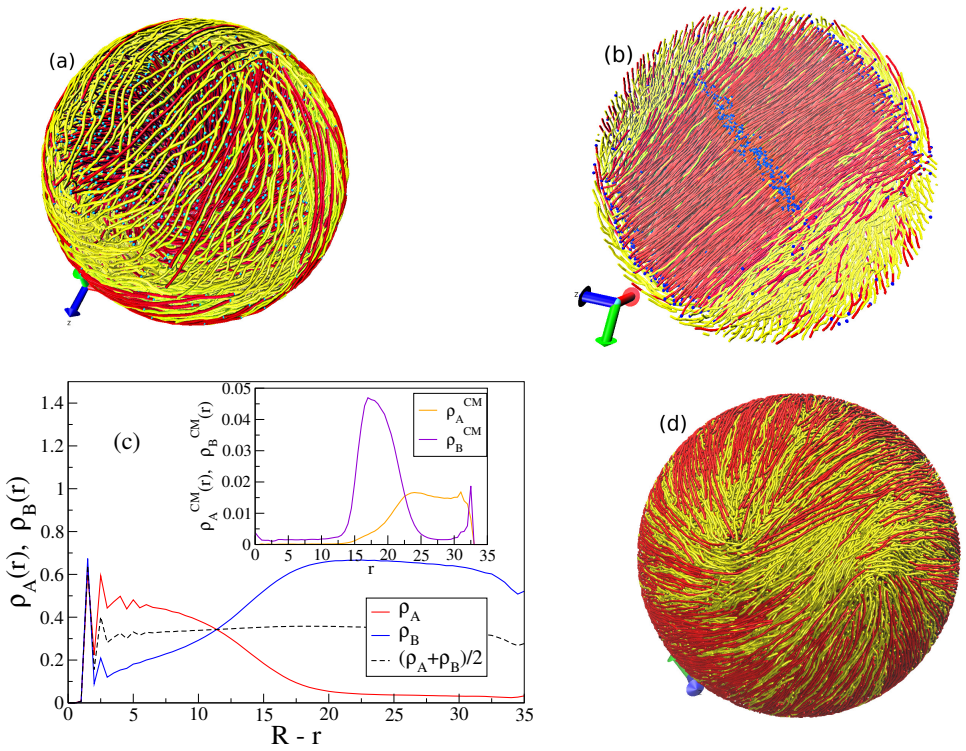

FIG. 13: Snapshot picture of chain configurations in a sphere of radius $R = 35$ at the density $\rho = 0.63$, for the case $N_A = N_B = 32, \kappa_A = 24, \kappa_B = 128, X_B = 0.5$, showing a side view from outside (a) and a cross-section (b). Chain ends of B-chains are marked in blue. c) Radial density profiles of the monomer densities and the total density for the case shown in panel a) d) Same as a), but for $R = 70$; note that 2 topological defects of "charge" $1/2$ can be recognized.

In this case ($R = 70$) only a more modest enrichment of B-chains in the center of the sphere could be detected, and the B-rich shell adjacent to the wall shows very strong layering. In all cases the local total density $\rho_A(r) + \rho_B(r)$ is found to stay approximately constant throughout the sphere, apart from the pronounced layering very close to the surface. For $R = 35$, however, the local density distribution shows a clear layered core-shell structure, with B-chains dominating both for $r < 20$ and right underneath the surface ($33 < r < 34$), while the A-chains dominate in between. Of course, the structure with the two quasi-smectic cylinders (Fig.13b) implies that A-chains near the center are removed almost completely while due to the cylindrical B-rich domains the enrichment of A-chains in the outer regions must be less perfect, due to the volume fraction "needed" by these cylinders.

These changes of structure formation also show up in the variation of the crossing points of radial A-B-density profiles in spherical confinement which we compare in Fig.14 with crossing points in the planar and cylindrical case (inset). In the latter case, only a single crossing point occurs: the stiffer chains are always enriched near the surfaces, the less stiff chains - away from it. In the case of spherical surfaces, and R not very large, A-chains are enriched near

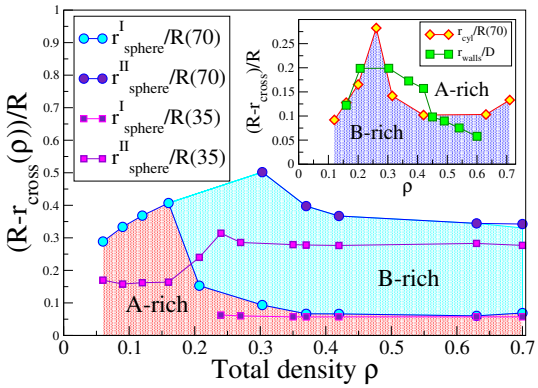

FIG. 14: Reduced distance $(R - r_{cross}(R))/R$ from the surface plotted versus density for $R = 35$ and $R = 70$ (main panel) and for the confinement in a cylinder with $R = 70$ (inset) and a planar slit (where the distance of the crossing point from the wall is normalized by half the slit thickness, $L_0 = D/2$), inset.

the surface for small densities, B-chains are enriched in the bulk. However, for large enough densities, there is always an enrichment of B very close to the wall, and then there are two crossing points, reflecting the fact that B-chains are predominant both near the center and very close to the wall.

So far the focus of our discussion has been to characterize the distributions of the densities $\rho_A(r), \rho_B(r)$ of the two species within the sphere, for a broad range of the average total density (from $\rho = 0.06$ to 0.63, Figs.3-12,13c). However, for densities $\rho = 0.2$ and larger the snapshot pictures of the chain conformations (e.g. Fig.7c, 13a-c) imply that a characterization of bond orientational order in these systems is worthwhile as well. Already in our earlier work on spherically confined single-component semiflexibe polymers we have seen that it is instructive to distinguish the behavior in a surface shell ($R - \delta < r < R$, with $\delta = 0.15R$) from the interior[14,15]. Here we follow this procedure but one has to distinguish also between the two components A and B.

The tensor Q in Eq.(3) has 3 eigenvalues $\lambda_1 < \lambda_2 < \lambda_3$: in an ideal uniaxial nematic structure, the largest eigenalue, $\lambda_3 = S$, yields the standard nematic order parameter (as shown already in Figs.10b, 11b); $\lambda_1 = \lambda_2 = -S/2$, and so the biaxiality $B = \lambda_2 - \lambda_1$ is then zero. For confined single-component systems it has been found that for some choices of stiffness a distinct biaxiality is present, and also the order parameter in the outer shell differs from its counterpart in the interior.

We have studied a possible biaxial order in the present system, recording the standard definition of biaxiality $B = \lambda_2 - \lambda_1$, both averaged over all bonds and separately for the A-chains and B-chains, exploring separately the interior and the outer region of the sphere, see Fig.15. However, contrary to what one might expect, the biaxiality of our chains induced by the curvature of the sphere surface is rather insignificant, it is never larger than just a few percent, cf. Fig.15b, and no interesting systematic trends can be recognized. Apparently, the additional degrees of freedom in our system (in comparison with the packaging of a single very long and very stiff chain in a sphere) allows a more homogeneous arrangement of the bond vectors in the polymer blend. Yet, Fig.15 demonstrates that for $\rho \geq 0.2$ the nematic ordering in the interior of the confined space for both A- and B-chains exceeds significantly that in the outer shell and deviates markedly from the average one throughout the sphere. One can also see that the B-chains

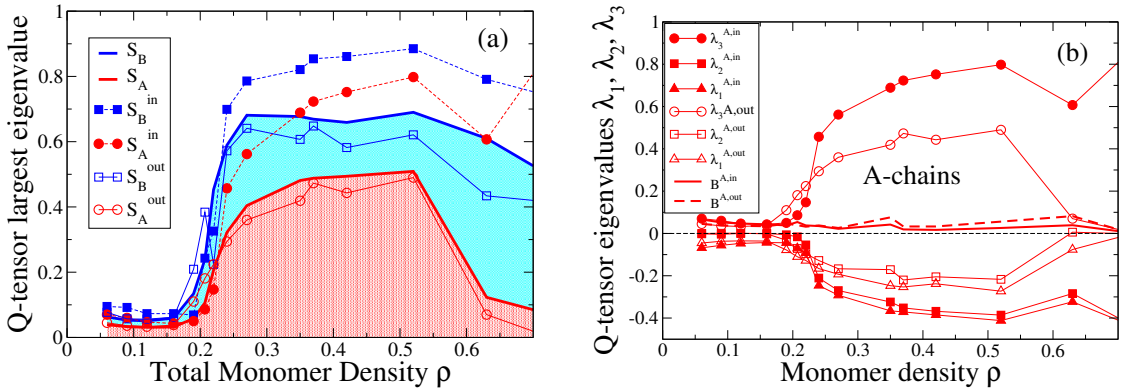

FIG. 15: (a) Variation of the nematic order parameters S_A, S_B with monomer density ρ, labeled as S_A^{in}, S_B^{in}, in the interior (shaded) region of the sphere $0 \le r \le 0.6R$), and as S_A^{out}, S_B^{out} in the outer one ($0.6R \le r \le R$). (b) Eigenvalues $\lambda_1, \lambda_2, \lambda_3$ of the Q-tensor vs density ρ for the A-chains in the interior (full symbols) and in the outer shell (empty symbols). The biaxiality parameter $B = \lambda_2 - \lambda_1$ marked by full/dashed line in/outside the region $0 \le r \le 0.6R$.

in the interior of the sphere are much better ordered than the A-chains for all densities exceeding 0.2. However, the A-chains are better ordered throughout the outer sphere than in the interior. In particular, for densities exceeding 0.5 the order of the A-chains in the interior of the sphere essentially disappears.

V. CONCLUSIONS

In this paper we have presented a study of the effect of sperical confinement on lyotropic solutions containing two types of semiflexible polymers which differ strongly in their chain stiffness, applying density functional theory (DFT) or Molecular Dynamics (MD) simulations. As emphasized in the introduction, such problems are relevant for applications in drug delivery where suitable polymers are encapsulated in vesicles, or in a biopolymer context (the classical example would be ds DNA and actin confined in cells). However, our modeling is restricted to highly simplified generic models, such as tangent hard sphere chains (studied by DFT) and simple bead-spring models (studied by MD), for which the phase diagram and physical properties of the polymers in bulk solution have been studied earlier in detail. For simplicity, equal chain lengths (mostly $N_A = N_B = 32$ beads) have been used, and persistence lengths (or stiffnesses κ_A, κ_B of the bond angle potential) $\kappa_A = 8$, $\kappa_B = 32$ (for the DFT work) and $\kappa_A = 24$, $\kappa_B = 128$ (for the MD work); note that our length unit is the bead diameter throughout. In the MD part, also the chain length dependence was briefly considered.

Increasing the monomer density ρ in the bulk solution for such systems, one finds an isotropic solution for small ρ, then an isotropic-nematic coexistence region, and finally for large enough ρ a nematic phase, where both constituents exhibit nematic order, irrespective of the mole fractions of the binary mixture X_A, X_B (with $X_A + X_B = 1$).

Spherical confinement in spheres with repulsive walls was studied for typical radii of $R = 35$ and $R = 70$ bead diameters, and whenever appropriate we have compared our results to corresponding data for cylinders (also with $R = 70$) and confinement in slit pores (with slit width $D = 128$). The reason for making such comparisons is that one expects strong effects when the radii are comparable to the contour length L of the stiff chains; in spheres with

$R \ll L$ clearly a strong distortion of the chain conformation would be inevitable, and for $R \gg L$ the behavior would only marginally differ from planar confinement of these polymers.

We have demonstrated that in all the studied cases there is a subtle interplay between the repulsive wall potential and entropic effects due to the mixing of the two constituents and the packing of the chains near the wall. In rather dilute systems, the average density near the wall is reduced. The stiffer species fits better to the confining surface, except for the smallest radius studied,$R = 35$, in the MD case. For denser systems, also for spheres there is always an enrichment of the stiffer chains very close to the surface, even though the stiffer chains are enriched near the sphere center as well. The average density stays always almost constant, apart from a depletion effect near the walls when the total monomer density in the system is small, and from wall induced layering when the density is large.

An interesting aspect that might deserve further investigation in the future is the local orientational order and composition in the neighborhood of the topological defects identified in the nematic order at the sphere surface for the dense systems. The precise characterization of vector fields near topological defects is a difficult problem of current interest[55], in particular also for active nematics[56] under confinement.

We note that a related entropy-induced separation has also been observed recently in simulations of confined mixtures of ring polymers[57]. In this work a rather small sphere, radius 20, containing both many short rings and a few, 10, long rings with length 50 was used. It was found that very stiff rings were also entropically attracted to the surface, compatible with what one would expect from our results. No nematic order was found in this system, as expected.

In experiments on solutions of DNA and actin filaments in micrometer scale vesicles[7] it was found that DNA was enriched near the surface, actin being dissolved in the central region of the sphere, while for small enough actin concentration also DNA was no longer attracted to the surface. Also DNA and alginate, which has only a persistence length of $5.7nm$[58], exhibit an interesting phase behavior in such micrometer scale confinement[58]. We hope that the present work will stimulate further experiments on suitable systems to study this interesting behavior.

Acknowledgments

We thank the German Research Foundation (DFG) for support under project numbers BI 314/24-2. The authors gratefully acknowledge the computing time granted on the supercomputer Mogon (hpc.uni-mainz.de). A.M. thanks the COST action No. CA17139, supported by COST (European Cooperation in Science and Technology) and its Bulgarian partner FNI/MON under KOST-11. We thank Dr.A. Nikoubashman for numerous stimulating and helpful

discussions.

References

[1] Alberts, B.; Johnson, A.; Lewis, J.; Raff, M.; Roberts, K.; Walker P. *Molecular Biology of the Cell* (Garland Science, New York, 2007)

[2] Earnshaw, W.; Harrison, S.; DNA arrangement in isometric phage heads. *Nature* **1977***, 268*, 598-602.

[3] Katzav, E.; Adda-Bedia, M.; Boudoud, A. A statistical approach to close packing of elastic rods and to DNA packaging in viral capsids. *PNAS* **2006***, 103*, 18900-18904.

[4] Soares e Silva, M.; Alvarado, J.; Nguyen, J.; Georouilla, N.; Mulder, B.; Koenderin, G. Self-organized patterns of actin filaments in cell-sized confinement. *Soft Matter* **2011***, 7*, 10631-10641

[5] Qi, W.; Yan, X.; Fei, J.; Wang, A.; Cui, Y.; Li, J. Triggered release of insulin from glucose-sensitive enzyme multilayer shells. *Biomaterials* **2009***, 30*, 2799-2806

[6] Wang, Y.; Wang, L.; Li, B.; Chang, Y.; Zhou, D.; Chen, X.; Jing, X.; Huang, Y. Compact Vesicles Self-Assembled from Binary Graft Copolymers with High Hydrophilic Fraction for Potential Drug/Protein Delivery. *ACS Macro Letters* **2017,** *6*, 1186-1190

[7] Negishi, M.; Sakaue, T.; Takiguchi, K.; Yoshikawa, K. Cooperation between giant DNA molecules and actin filaments in a microsphere. *Phys. Rev. E* **2010***, 81,* 051921

[8] McIntosh, D. B.; Ribeck, N.; Saleh, O. A. Detailed scaling analysis of low-force polyelectrolyte elasticity, *Phys. Rev. E* **2009***, 80*, 041803

[9] Purdy, K. R.; Varga, S.; Galindo, A.; Jackson, G.; Fraden, S. Nematic Phase Transitions in Mixtures of Thin and Thick Colloidal Rods. *Phys. Rev. Lett.* **2005***, 94*, 057801.

[10] Ciferri, A.; Krigbaum, W. R.; Meyer, R. B. *Polymer Liquid Crystals* (Academic Press , New York, 1982)

[11] A. Ciferri (ed.) *Liquid Crystallinity in Polymers* (VCH Publ. , New York, 1991)

[12] Donald, A. M.; Windle A. H.; Hanna, S. *Liquid Crystalline Polymers* (Cambridge University Press, Cambridge, 2006)

[13] Binder, K.; Egorov, S. A.; Milchev A.; Nikoubashman, A. Understanding the Properties of Liquid-Crystalline Polymers by Computational Modeling. *J. Phys. Materials* **2020***, 3*, 032008

[14] Nikoubashman, A. ; Vega, D. A.; Binder, K.; Milchev, A. Semiflexible Polymers in Spherical Confinement: Bipolar Orientational Order Versus Tennis Ball States. *Phys. Rev. Lett.* **2017***, 118,* 217803

[15] Milchev, A.; Egorov, S. A.; Vega, D. A.; Binder, K.; Nikoubashman, A. Densely Packed Semiflexible Macromolecules in a Rigid Spherical Capsule. *Macromolecules* **2018***, 51*, 2002-2016.

[16] Hoffmann K. B.; Sbalzarini, I. F. Robustness of topological defects in discrete domains. *Phys.Rev. E* **2021***, 103*, 012602

[17] Petrov, A. S.; Boz, M. B.; Harvey, S. C. The conformation of double-stranded DNA inside bacteriophages depends on capsid size and shape. J. Struct. Biol. **2007**, 160, 241-248.

[18] Locker, C. R.;Fuller, S. D.; Harvey, S, C. DNA organization and thermodynamics during viral packing. Biophys. J. **2007**, 93, 2861-2869.

[19] Shin, H.; Grason, G. M. Filling the void in confined polymer nematics: Phase transitions in a minimal model of dsDNA

packing. Europhys. Lett. **2011**, 96, 3600.

[20] Liang, Q.; Jiang, Y.; Chen, J. Z. Y. Orientationally ordered states of a wormlike chain in spherical confinement Phys. Rev. E **2019**, 100, 032502.

[21] Curk, T.; Farrell, J. D.; Dobnikar, J.; Podgornik, R. Spontaneous Domain Formation in Spherically Confined Elastic Filaments. Phys. Rev. Lett. **2019**, 123, 047801.

[22] Zandi, R.; Dragne, B.; Travesset, A.; Podgornik, R. On virus growth and form. Physics Reports **2020**, 847, 1-102.

[23] Dutta, D.; Fruitwala, H.; Kohli, A.; Weiss, R. A. Polymer blends containing liquid crystals: A Review. *Polym. Eng. Sci.* **1990***, 30*, 1005.

[24] Semenov A. N.; Subbotin, A. V. Phase equilibria in mixtures of rigid chain polymers. *Polym. Sci. U.S.S.R.* **1989***, 31*, 2266-2273.

[25] Dennison, M.; Dijkstra, M.; van Roij, R. The effects of shape and flexibility on bio-engineered fd-virus suspensions. *J. Chem. Phys.* **2011***, 135*, 144106

[26] Milchev, A.; Egorov, S. A.; Midya, J.; Binder, K.; Nikoubashman, A. Entropic Unmixing in Nematic Blends of Semiflexible Polymers. *ACS Macro Lett.* **2020***, 9*, 1779-1784.

[27] Egorov, S. A.; Milchev, A.; Nikoubashman, A.; Binder, K. Phase Separation and Nematic Order in Lyotropic Solutions: Two Types of Polymers with Different Stiffnesses in a Common Solvent. *J. Phys. Chem. B* **2021)***, 125*, 956969.

[28] Sato T.; Teramoto, A. Concentrated solutions of liquid-crystalline polymers. *Adv. Polym. Sci.* **1996***, 126,* 85-161.

[29] Reisner, W.; Pedersen J. N.; Austin, R. H. DNA confinement in nanochannels: physics and biological applications. *Rep. Progr. Phys.* **2012***, 75*, 106601

[30] Kumar, S. K.; Yethiraj, A.; Schweizer, K. S.; Leermakers, F. A. M. The effects of local stiffness disparity on the surface segregation from binary polymer blends. *J. Chem. Phys.* **1995***, 103*, 10332-10346.

[31] Jung, Y.; Kim, J.; Jun, S.; Ha, B.-Y. Intrachain Ordering and Segregation of Polymers under Confinement. Macromolecules **2012**, 45, 32563262.

[32] Ha, B-Y.; Jung, Y.; Polymers under confinement: single polymers, how they interact, and as model chromosomes. Soft Matter **2015**, 11, 2333-2352.

[33] Kremer K. Grest, ; G. S. Dynamics of entangled linear polymer melts: A moleculardynamics simulation. *J. Chem. Phys.* **1990***, 92*, 5057.

[34] Milchev, A.; Egorov, S. A.; Binder, K.; Nikoubashman, A. Nematic order in solutions of semiflexible polymers: Hairpins, elastic constants, and the nematic-smectic transition. *J. Chem. Phys.* **2018***, 149*, 174909

[35] Milchev, A.; Egorov, S. A.; Nikoubashman, A.; Binder, K. Conformations and orientational ordering of semiflexible polymers in spherical confinement. *J. Chem. Phys.* **2017***, 146*, 194907

[36] Allen M. P.; Tildesley, D. J. *Computer Simulation of Liquids*, 2nd. ed. (Oxford University Press, Oxford, 2017)

[37] Anderson, J.; Lorenz, C.; Travesset, A. General purpose molecular dynamics simulations fully implemented on graphics processing units. *J. Comput. Phys.* **2008***, 227*, 5342-5359.

[38] Glaser, J.; Nguyen, T. D.; Anderson, J. A.; Liu, P.; Spiga, F.; Millan, J. A.; Morse, D. C.; Glotzer, S. C. Strong scaling of general-purpose molecular dynamics simulations on GPUs. *Comput. Phys. Commun.* **2015***, 192*, 97-107.

[39] Fynewever H.; Yethiraj, A. Phase behavior of semiflexible tangent hard sphere chains. *J. Chem. Phys.* **1998***, 108*, 1636.

[40] Egorov, S. A.; Milchev, A.; Binder, K. Anomalous Fluctuations of Nematic Order in Solutions of Semiflexible Polymers.

Phys. Rev. Lett. **2016**, *116*, 187801.

[41] Guggenheim, E. A. Statistical thermodynamics of the surface of a regular solution. *Trans. Faraday Soc.* **1945**, *41*, 150.

[42] Egorov, S. A.; Milchev, A.; Virnau, P.; Binder, K. Semiflexible polymers under good solvent conditions interacting with repulsive walls. *J. Chem. Phys.* **2016**, *144*, 174902.

[43] Kratky O.; Porod, G. Röntgenuntersuchung gelöster Fadenmoleküle. *Recl. Trav. Chim.* **1949**, *68*, 1106.

[44] Stoop, N.; Najafi, J.; Wittel, F. K.; Habibi, M.; Herrmann, H. J. Packing of Elastic Wires in Spherical Cavities. *Phys. Rev. Lett.* **2011**, *106*, 214106.

[45] Fathizadeh, A.; Heidari, M.; Eslami-Mossallam, B.; Ejtehadi, M. R. Confinement dynamics of a semiflexible chain inside nano-spheres. *J. Chem. Phys.* **2013**, *139*, 044912.

[46] Milchev A.; Binder, K. Cylindrical confinement of solutions containing semiflexible macromolecules: surface-induced nematic order versus phase separation. *Soft Matter* **2021**, *17,* 3443.

[47] van Roij, R.; Dijkstra, M.; Evans, R. Interfaces, wetting, and capillary nematization of a hard-rod fluid: Theory for the Zwanzig model. *J. Chem. Phys.* **2000**, *113*, 7689.

[48] Chen, J. Z. Y.; Sullivan, D. E.; Yuan, X. Surface-Induced Liquid Crystal Transitions of Wormlike Polymers Confined in a Narrow Slit. A Mean-Field Theory. *Macromolecules* **2007**, *40*, 1187.

[49] Ivanov, V. A.; Rodionova, A. S.; An, E. A.; Martemyanova, J. A.; Stukan, M. R.; Müller, M.; Paul,W.; Binder, K. Orientational ordering transitions of semiflexible polymers in thin films: A Monte Carlo simulation. *Phys. Rev. E* **2011**, *84*, 041810.

[50] Ivanov, V. A.; Rodionova, A. S.; Martemyanova, J. A.; Stukan, M. R.; Müller, M.; Paul, W.; Binder, K. Wall-induced orientational order in athermal semidilute solutions of semiflexible polymers: Monte Carlo simulations of a lattice model. *J. Chem. Phys.* **2013**, *138*, 234903.

[51] Ye, S.; Zhang, P.; Chen, J. Z. Y. Surface-induced phase transitions of wormlike chains in slit confinement. *Soft Matter* **2016**, *12*, 2948-2959.

[52] Zhang, W.; Gomez, E. D.; Milner, S. T. Surface-induced chain alignment of semiflexible polymers. *Macromolecules* **2016**, *49*, 963-971.

[53] Luzhbin D. A.; Chen, Y.-L. Shifting the IsotropicNematic Transition in Very Strongly Confined Semiflexible Polymer Solutions. *Macromolecules* **2016**, *49*, 6139-6147.

[54] Egorov, S. A.; Milchev, A.; Binder, K. Capillary Nematization of Semiflexible Polymers. *Macromol. Theory Simul.* **2017**, *26*, 1600036.

[55] Hoffmann K. B.; Sbalzarini, I. F. Robustness of topological defects in discrete domains. *Phys. Rev. E* **2021**, *103*, 012602.

[56] Keber, F. C.; Loiseau, E.; Sanchez, T.; De Camp, S. J.; Giomi, L.; Bovick, M. J.; Marchetti, M. C.; Dogic, Z.; Bausch, A. R. Topology and dynamics of active nematic vesicles. *Science* **2014**, *345*, 1135.

[57] Zhou, X.; Guo, F.; Li, K.; He, L.; Zhang, L. Entropy-Induced Separation of Binary Semiflexible Ring Polymer Mixtures in Spherical Confinement. *Polymers* **2019**, *11*, 1992.

[58] Negishi, M.; Ichikawa, M.; Nakajima, M.; Kojima, M.; Fukuda, T.; Yoshikawa, K. Phase behavior of crowded like-charged mixed polyelectrolytes in a cell-sized sphere. *Phys. Rev. E* **2011**, *83*, 061921.

for Table of Contents use only